

Metal-enhanced fluorescence from thermally stable rhodium nanodeposits

Yongxia Zhang^a and Chris D. Geddes^{*b}

Received 7th June 2010, Accepted 15th July 2010

DOI: 10.1039/c0jm01806f

Different density rhodium nanoparticulate substrates were fabricated by electron-beam physical vapor deposition in order to study the fluorescence of close-proximity fluorophores to the high thermally stable rhodium nanoparticles. We observed an apparently constant metal-enhanced fluorescence (MEF), when fluorophores were placed in close proximity to rhodium nanoparticles before and after autoclaving of the substrates. Fluorophores with different emission wavelength maxima and free-space quantum yields have also been studied and can undergo different enhancements, a 2.5-fold increase in far-field luminescence was observed from 15 nm Rh films for Tinopal, and up to a 10-fold enhancement was observed for fluorescein. Similarly, the *near-field* fluorescence enhancement values were estimated to be ~125 and 500 fold, respectively. Further, the electromagnetic field distributions around different size Rh nanoparticles were simulated using FDTD to understand the wavelength dependence of the e-field. Our findings show that the decay time of fluorophores was not reduced near to the rhodium substrates, suggesting only an enhanced electric field component is the mechanism for fluorescence enhancement.

1. Introduction

Fluorescent probes are widely used to detect specific targets in medical diagnostics, high-throughput screening, microscopy and in a plethora of other biotechnology applications today.^{1–4} While fluorescence spectroscopy displays exquisite sensitivity,^{1,5,6} the detection limit of classical fluorescence is still limited by the quantum yield of the fluorophore, the autofluorescence of the sample and the photostability of the fluorophores, which are fundamentally far-field fluorescence properties.⁷ In this regard, metallic nanostructures^{8–11} have been used to favorably modify the spectral properties of fluorophores in the near-field and to favorably alter some of their more classical photophysical far-field constraints.^{12–22} Fluorescence enhancement has been studied for many years for fluorophores close to metallic nanoparticles. The use of fluorophore–metal near-field interactions has been termed metal-enhanced fluorescence (MEF)^{23–26} by Geddes. To date, MEF from plasmonic nanostructured materials such as silver,^{24,27} gold,²⁸ copper,²⁹ zinc,³⁰ chromium,³¹ nickel,³² tin³³ and iron³² have been observed by our lab. However, all of these metals have poor thermal³⁴ and chemical stability. Subsequently, there are many potential advantages of using rhodium substrate for MEF: (1) rhodium is a hard silvery white and durable metal which has high reflectance, (2) rhodium metal does not normally form an oxide, even when heated, (3) rhodium has high chemical stability and the surfaces containing small rhodium particles are expected to be stable indefinitely and (4) rhodium is not easily corroded and etched by acids.

In this paper, we present experimental and theoretical data for rhodium structures to investigate whether they are suited for MEF temperature independent applications. Rhodium

nanodeposits were fabricated by electron-beam physical vapor deposition,³⁵ which were subsequently characterized by optical absorption spectroscopy and Atomic Force Microscopy (AFM) techniques. Significantly enhanced fluorescence emission was observed when fluorophores were positioned near to the rhodium structures. In addition, we have observed similar MEF both before and after the heat treatment (autoclaving) of rhodium slides, suggesting their use in temperature measurements or as an autoclavable MEF substrate. With regard to the actual MEF mechanism for Rh substrates, we have not observed a shorter fluorescence lifetime for close-proximity fluorophores, which suggests that only an enhanced electric field underpins the mechanism for fluorescence enhancement.

2. Experimental section

2.1 Materials

Fluorophores: fluorescein was obtained from Sigma-Aldrich Chemical company and Tinopal CBS was purchased from TCI. They were used as received. Blue chemiluminescence dye was obtained from Unique Ind. Inc., Philadelphia, PA, USA. Silane-prepTM glass microscope slides were purchased from Sigma-Aldrich. Rhodium nanostructured films of various thicknesses were deposited onto Silane-prepTM glass microscope slides using e-beam deposition.

2.2 Fabrication of Rh nanodeposits by electron-beam physical vapour deposition

Rhodium thin films were deposited in a stainless steel chamber, which was pumped and the pressure was 6×10^{-6} Torr. The thickness monitor was set up for desired thickness (1, 3, 5, 7 and 10 nm). The high D.C. voltage (30 kilovolts) was applied on. The Rh crucible was heat up and Rh was evaporated and deposited on substrates.

^aInstitute of Fluorescence, University of Maryland, Baltimore County, 701 East Pratt St, Baltimore, MD, 21202, USA

^bInstitute of Fluorescence and Department of Chemistry and Biochemistry, University of Maryland, Baltimore County, 701 East Pratt Street, Baltimore, MD, 21202, USA. E-mail: geddes@umbc.edu

2.3 Preparation of sandwich format samples for metal-enhanced fluorescence measurements

A solution of 60 μL of fluorophore (500 nM) was sandwiched between two glass slides for the control sample and between one glass and one rhodium nanostructured film. The dye was excited with a 473 nm laser line source and the fluorescence emission spectra were collected after passing through a 473 nm notch filter.

2.4 Heat treatment of rhodium slides

One rhodium slide was placed in a glass beaker and the beaker was covered with foil. A dry cycle was used at temperatures around 120 $^{\circ}\text{C}$. After autoclaving the samples were stored under vacuum until the spectroscopic measurements were undertaken.

2.5 Optical spectroscopy

The absorption spectra of the rhodium nanostructured films of varying thicknesses were collected using a Varian Cary 50 UV-Vis spectrophotometer. Fluorescence spectra of the fluorophores were measured with blank glass sandwiches (control samples) and glass–nanostructured film sandwiches (MEF substrates) using an Ocean Optics HD2000 fluorometer and Varian Cary Eclipse Fluorescence spectrophotometer.

2.6 Time-domain fluorescence lifetime measurements

Time-domain lifetime measurements of the fluorophores were measured in a cuvette (solution), glass slide sandwiches, and glass–rhodium substrate sandwiches in a front-face 45 $^{\circ}$ geometry using a Horiba Jobin Yvon TemPro system with pulsed laser diodes for excitation, filters and a TBX4 module for emission detection. The data were fitted to single exponential decay kinetics using impulse reconvolution analysis and a χ^2 goodness of fit criterion.

2.7 Atomic force microscopy (AFM)

AFM images were performed on a Molecular Imaging Picoplus Microscope. Samples were imaged at a scan rate of 1 Hz with 512 \times 512 pixel resolution in a tapping mode.

2.8 FDTD calculations

The FDTD method was employed to determine the relative electric field intensities and distributions at the surface of rhodium nanoparticles in a Total Field Scattered Field (TFSF), recalling that an enhanced e-field is one of the two mechanisms thought to contribute to fluorescence enhancement in MEF. TFSF sources are used to divide the computation area or volume into total field (incident plus scattered field) and scattered field only regions.^{36,37} The incident p-polarized electric field is defined as a plane wave with a wavevector that is normal to the injection surface (denoted by the white arrow in Fig. 9). The scattered and total fields were monitored during the simulation such that the total or scattered transmission can be measured. Using Lumerical FDTD Solution software, for different size particle simulation, the particle size was set to 1, 5, 10, and 50 nm diameter, respectively. The simulation region was set to 600 \times 600 nm with

a mesh accuracy of 5. The overall simulation time was set to 200 fs and calculated over a wavelength range from 200–800 nm for the rhodium nanoparticles of different sizes (1, 5, 10 and 50 nm).

3. Results and discussion

Fig. 1 left shows the photograph of Rh metal pellets and Rh nanostructure deposited slides with different thicknesses 1, 3, 5, 7, 10 and 15 nm, demonstrating the semi-transparent nature of the Rh films, allowing one to see their optical transparency as a function of decreased loading. Absorption spectra of e-beam deposited metallic Rh of various thicknesses deposited onto glass slides are shown in Fig. 1, which shows that there is no absorption peak for 1, 3, 5, 7, 10 and 15 nm thick Rh films in the range of 300–800 nm. The AFM images of 1, 3, 5, 7, 10 and 15 nm Rh films are shown in Fig. 2. For the 1 nm rhodium film, we observe separated islands with a height of ~ 0.7 nm, as seen from the line scan results. For the 3 nm rhodium film, the height of the separated islands is ~ 2 nm. It can be concluded from the AFM images that for 1, 3, 5, 7 and 10 nm Rh samples, only one layer of separated Rh islands (similar to separated Rh nanoparticles) was formed on the glass slides due to the height of the islands being close to the Rh film thickness measured by the Quartz Crystal Microbalance (QCM), which measures a mass per unit area by measuring the change in frequency of a quartz crystal resonator in the e-beam vacuum deposition chamber. However, for the 15 nm Rh film, the height of the most separated islands was around 4 nm, which was much lower than the thickness of the Rh film measured by QCM in the evaporator, which suggests that there are multiple layers of Rh nanoparticles on the slide. The surface roughness was also measured using AFM. The surface roughness S_n is defined by the following expression:

$$S_n = \frac{1}{n} \sum_{i=1}^n |f(x_i, y_i) - \langle f_n \rangle| \quad (1)$$

where $\langle f_n \rangle$ is an average value of sampling $f(x_i, y_i)$ and n is the sampling volume.

$$\langle f_n \rangle = \frac{1}{n} \sum_{i=1}^n |f(x_i, y_i)| \quad (2)$$

The roughness of 1, 3, 5, 7, 10 and 15 nm rhodium slides is 0.257, 0.25, 0.17, 0.233, 0.83, and 0.9 nm, respectively. We observed that the roughness is increased with an increased Rh thickness above 5 nm.

The fluorescence emission spectra of fluorescein on different thickness of Rh films and on glass are shown in Fig. 3. It can be seen that the fluorescence of fluorescein is enhanced (~ 10 fold) for 15 nm Rh, as compared to the glass control sample *i.e.* no metal, with the enhancement factor increasing with an increased Rh thickness. It is somewhat easy to understand this trend where from 1 to 10 nm, the enhancement factor is increased with increased surface roughness. We estimate the distance between a pair of sandwich slides to be ~ 1 μm , and in this geometry only $\sim 2\%$ of the solution is believed to be in the plasmon enhancing near-field range.²³ This suggests the near-field enhancement factor is ~ 500 fold on the 15 nm rhodium slide, which downstream lends itself to a 10-fold enhancement in far-field fluorescence.

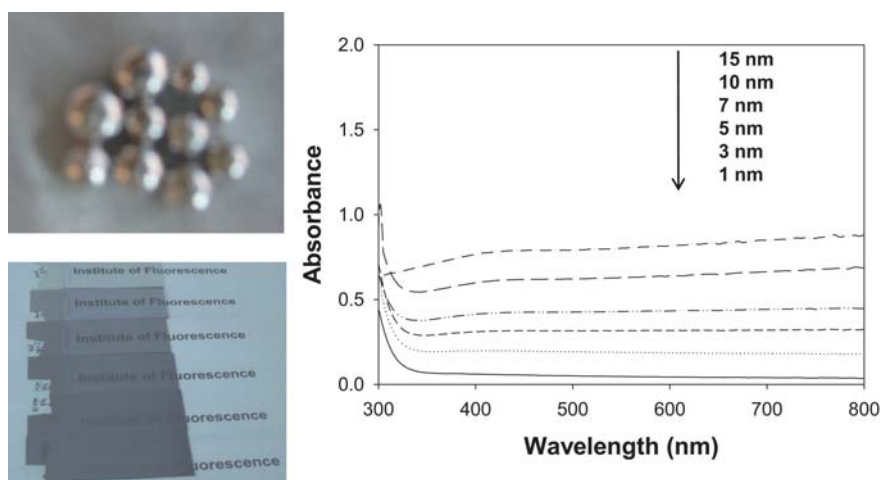


Fig. 1 Photograph of Rh metal pellets and Rh nanostructure deposited slides with different thicknesses 1, 3, 5, 7, 10 and 15 nm, demonstrating the semi-transparent nature of the Rh films (left). Absorption spectrum of vapor deposited metallic Rh of various thicknesses deposited onto glass slides (right).

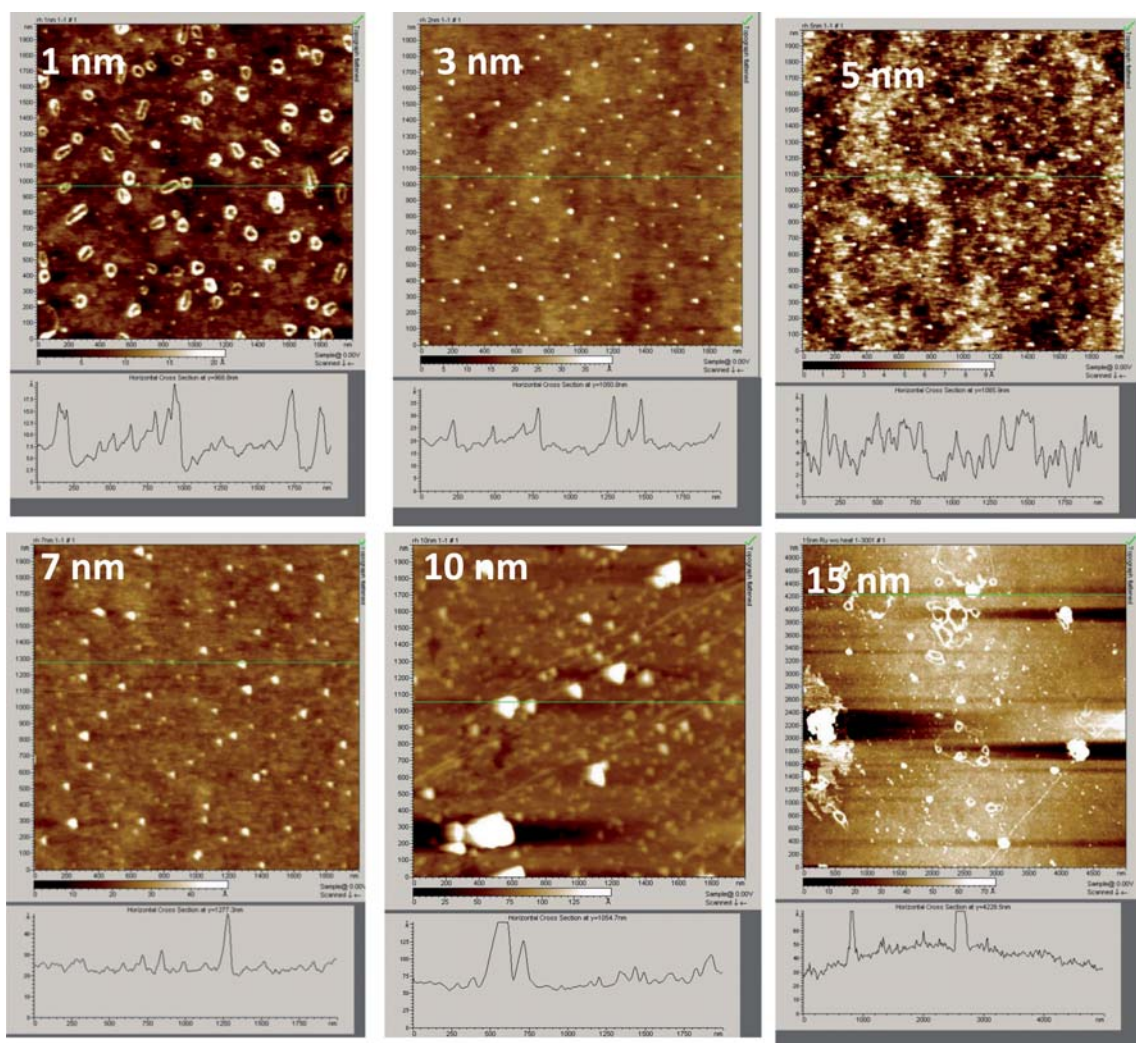


Fig. 2 AFM images of 1, 3, 5, 7, 10 and 15 nm Rh on glass. Below are the respective line scans of the AFM images.

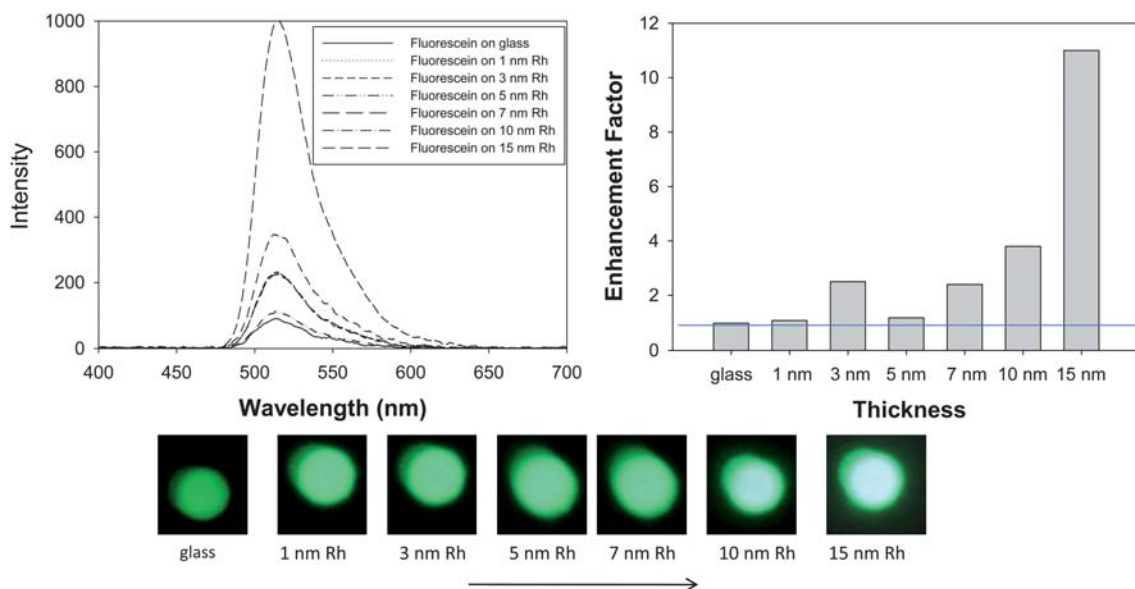


Fig. 3 Emission spectra and fluorescence enhancement factor for a solution of fluorescein in water sandwiched between glass and Rh slides of varying thicknesses. The enhancement factors were determined from several measurements on the film surface. G–G: glass sandwich control sample (top). Real color photographs of emission were taken through a 473 nm notch filter (bottom).

In order to test the thermal stability of Rh deposited slides for MEF applications, Rh deposited slides were autoclaved for 45 min at $\sim 120^\circ\text{C}$. Fig. 4 shows photographs and AFM images of 15 nm Rh before and after the autoclave procedure. Visually the Rh slides look identical. Additionally from the AFM images, the morphologies and the roughnesses are also very similar, slight differences being due to the inherent difficulty of imaging the exact same region on the slide. We then compared the fluorescein emission both before and after heating. In contrast, silver particulate films after thermally annealing, non-, *just*-, and thick continuous silver films, show significant changes in the AFM morphology, free-space absorption and emissive properties of close-proximity fluorophores with temperatures $> 80^\circ\text{C}$ showing a notable effect.³⁸ Subsequently, our results suggest that rhodium slides are good candidates for thermally stable MEF applications.

In addition, the fluorescence emissions of Tinopal CBS on different thickness Rh films/quartz and between two quartz slides (control sample) were investigated as shown in Fig. 5. It can be seen that the fluorescence of Tinopal CBS is enhanced (2.5 fold) on 15 nm Rh, as compared to the quartz control sample *i.e.* no metal, with a similar trend in enhancement factor as observed for fluorescein, *i.e.* with increased Rh thickness (1–15 nm). This finding suggests MEF is both wavelength and quantum yield dependent (the emission peak of Tinopal CBS is ~ 440 nm; the emission peak of fluorescein is ~ 513 nm) similar to that reported for silver nanoparticles³⁹ and indeed for a whole range of other metals.⁴⁰

The time-reduced intensity decays (fluorescence lifetimes) of fluorescein near to rhodium substrates were also measured. The overall results of the lifetime analysis are given in Table 1. The decay curves of fluorescence between glass–glass sandwiches and

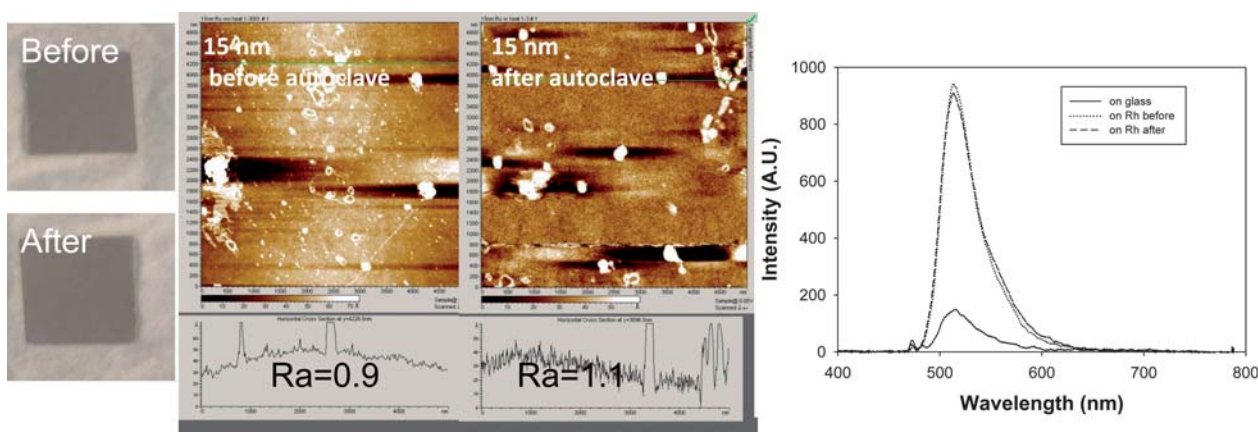


Fig. 4 Photograph and AFM images of Rh 15 nm nanostructure deposited slides before and after autoclave. Fluorescence emission spectra of fluorescein from 15 nm Rh with and without autoclave.

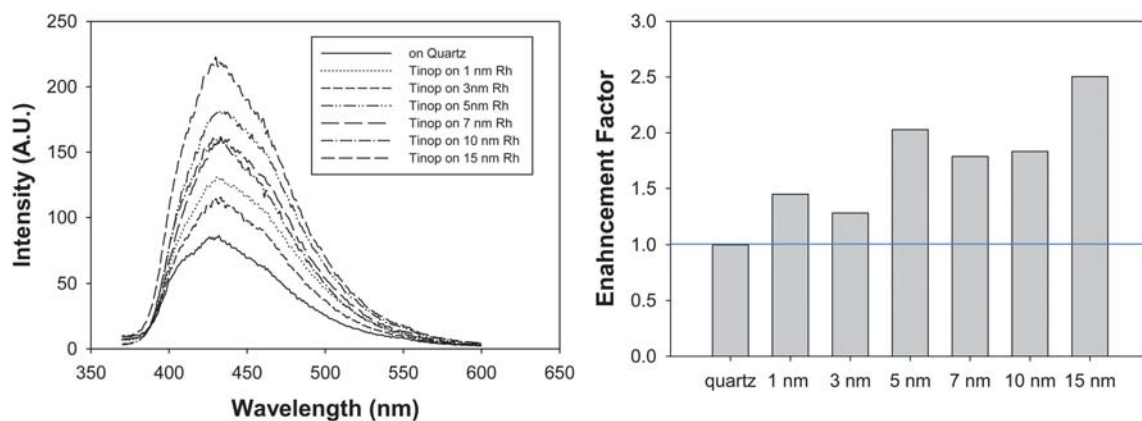


Fig. 5 Emission spectra and fluorescence enhancement factor for a solution of Tinopal CBS in water sandwiched between glass and Rh slides of varying thicknesses. The enhancement factors were determined from several measurements on the film surface. G–G: glass sandwich control sample.

Table 1 Fluorescence lifetime of fluorescein in water and on Rh nano-deposits measured using time-domain fluorometry. $\langle\tau\rangle$: the amplitude-weighted lifetime. $\bar{\tau}$: the mean lifetime

	τ /ns	A_1 (%)	$\langle\tau\rangle$ /ns	$\bar{\tau}$ /ns	χ^2
Fluorescein in H ₂ O in cuvette	3.9	100	3.9	3.9	1.0
Fluorescein glass/glass sandwich	3.9	100	3.9	3.9	1.0
Fluorescein X nm Rh/glass	3.9	100	3.9	3.9	1.0

between glass and different thickness Rh sandwiches are shown in Fig. 6. The decay curves were fitted to single-exponential decay kinetic functions with impulse reconvolution analysis and a χ^2 goodness of fit criterion. The lifetime of fluorescein on glass substrates is identical to that for fluorescein in a cuvette (lifetime of fluorescein in bulk solution is 3.9 ns in a solution in cuvette and on glass slides). In addition, we observed that the lifetime of the fluorophore–metal system was also 3.9 ns on glass/rhodium.

Over the last several years, we have proposed two complementary and cumulative effects for the fluorescence

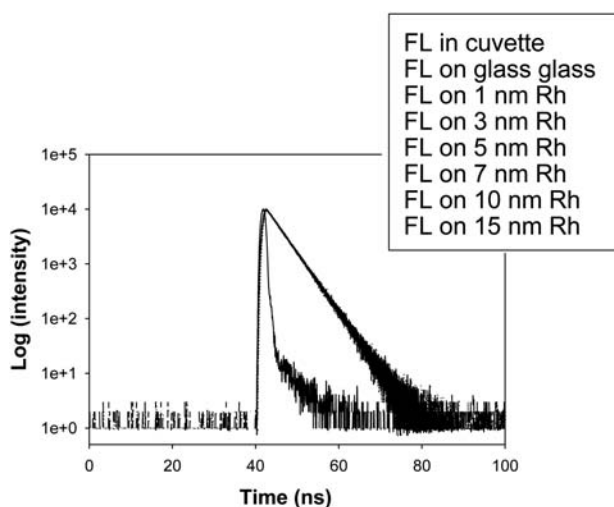


Fig. 6 Fluorescence intensity decays of fluorescein from glass–glass and different thicknesses of Rh–glass slides.

enhancement for fluorophores in close proximity to metallic nanoparticles:^{38,39} (i) surface plasmons can radiate coupled-fluorescence efficiently which underpins the generally observed shorter lifetime (enhanced photostability) and (ii) an enhanced absorption or electric field also facilitates enhanced emission. For Rh, there is no lifetime decrease on Rh slides, which suggests the enhanced fluorescence solely originates from the enhanced electric field, a similar result to that observed from chromium nanodeposits.³¹

In this regard, we have also investigated fluorophore photostability on rhodium nanoparticles. In Fig. 7, the intensity vs. time (photostability) of fluorescein on a 15 nm Rh film and on glass is shown. The figure shows fluorescein emission as a function of time, excited at 473 nm and observed using a 473 nm notch filter. The relative magnitudes of the intensity decays reflect that more detectable photons can be observed per unit time from the 15 nm Rh film, as compared to glass (a control sample), where the integrated areas under the plots is proportional to the photon flux from the respective samples. By additionally adjusting the laser power (using a neutral density filter) to match the initial steady-state intensities of the samples, the fluorescein on Rh can be seen to have similar photostability. This

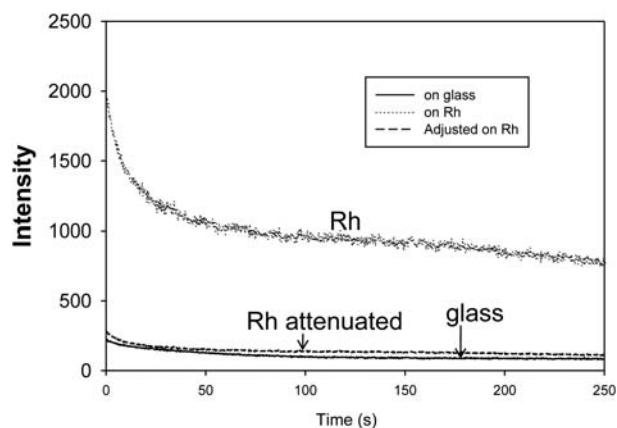


Fig. 7 Emission intensity vs. time (photostability) of fluorescein on 15 nm Rh films and glass, and with the laser power adjusted to give the same initial steady-state fluorescence intensity as observed on glass.

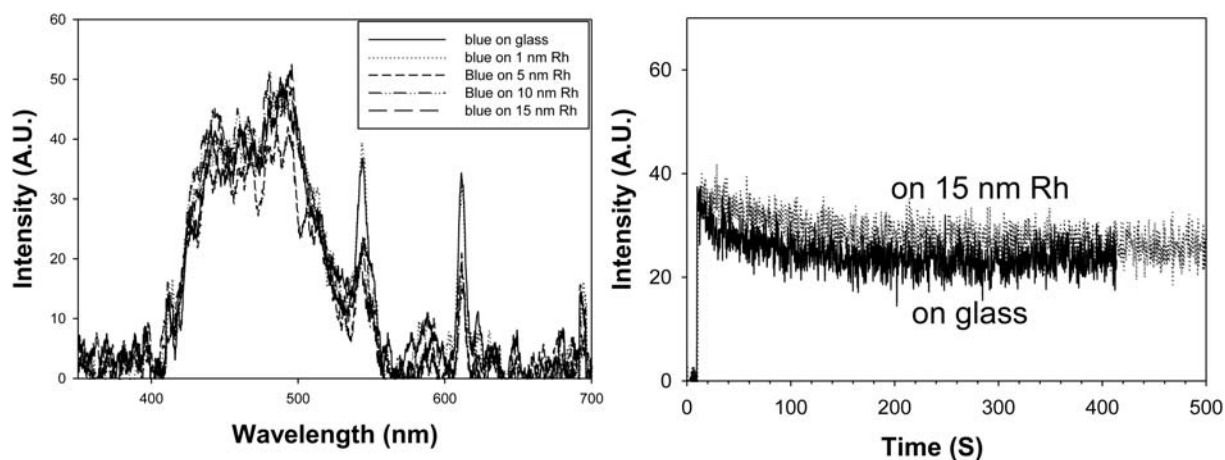


Fig. 8 Blue chemiluminescence emission from both glass and different thickness Rh surfaces (left). Chemiluminescence intensity decay measured on both Rh and glass as a function of time (right).

finding is consistent with the fact that the lifetime of the fluorescein is similar on a 15 nm Rh film as compared to that observed on glass, where a decreased lifetime lends itself to enhanced fluorophore photostability.⁴⁰

In order to further understand the mechanism of metal enhanced fluorescence from Rh nanodeposits, which is assumed only due to the enhanced electric field effect and, not surface Plasmon coupling, we studied whether there is metal-enhanced chemiluminescence (MEC)^{41,42} on Rh slides, where surface plasmons can be directly excited by chemically induced electronically excited near-field molecules, a phenomenon which is readily observed from silver nanodeposited surfaces.

Subsequently we measured blue chemiluminescence on glass and from Rh slides. Fig. 8 shows the blue chemiluminescence emission spectra from between the Rh/glass and glass plates, which reveals that there is no MEC from the Rh surfaces. Also, we measured the luminescence intensity as a function of time (chemiluminescence decay). Interestingly, the luminescence from the Rh surface is similar to the initial intensity on glass. The rates of loss of chemiluminescence were also similar on glass and Rh. This observation confirms there is no surface plasmon coupling component in the MEF mechanism for rhodium nanodeposits and suggests that the enhanced fluorescence observations are due to an enhanced near-field e-field.

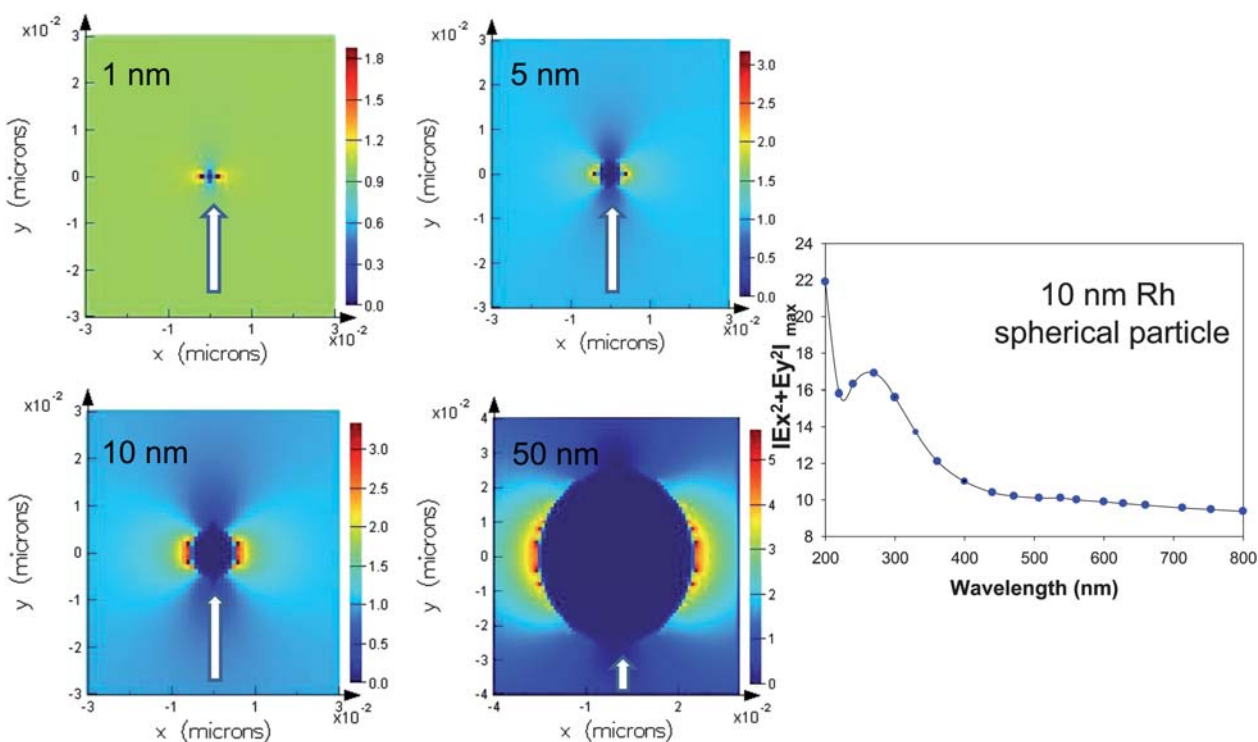


Fig. 9 Images of near-field intensity distributions around 1, 5, 10, and 50 nm Rh nanoparticles with 472 nm incident light. White arrow shows direction of the incident light injection at 472 nm. Calculations were undertaken using FDTD (left). The wavelength dependence of electric field ($|E_x^2 + E_y^2|$) maximum intensity for a 10 nm Rh nanoparticle (right).

Given that the mechanism is subsequently underpinned by an enhanced electric field component, we have simulated the electromagnetic field around different size Rh nanoparticles to understand the spatial distributions of the fields using FDTD calculations (Fig. 9). Using Lumerical (Canada) FDTD Solution software, the experimental simulation region was set to 600×600 nm with a mesh accuracy of 5. The overall simulation time was set to 200 fs and calculated over a wavelength range of 200–800 nm for Rh nanoparticles. In this FDTD calculation, we have chosen 1, 5, 10, and 50 nm diameter particles to show the electric field trends with incident light at 472 nm as a function of size. For 10 nm Rh nanoparticles, FDTD calculations revealed that the maximum electric field intensity is predicted to occur over a range of wavelengths in the ~ 200 to 300 nm range. This suggests that Rh nanoparticles will enhance fluorescence signatures well over this wavelength range, much better than the values we have obtained for both Tinopal and fluorescein in the visible portion of the emission spectrum.

Conclusions

In this paper we have studied the effects of rhodium nanoparticles on near-field fluorescence. We conclude that rhodium nanoparticles with high thermal stability can enhance the intensity of fluorophores. In addition, fluorophores with different emission wavelength maxima and free-space quantum yields in close proximity to rhodium nanoparticles can undergo different absolute enhancements. Furthermore, the decay time of fluorophores was observed the same *near to* the Rh substrates, suggesting only an enhanced electric field is the mechanism for fluorescence enhancement, with no plasmon-coupling component, as also verified by using chemiluminescence solutions, where no electric field component is present, *i.e.* no external source. Finally, of particular importance in this study is the fact rhodium deposited substrates do not show any temperature dependence on both their surface morphology and also their downstream near-field interactions with fluorophores after being exposed to autoclaving temperatures. This finding is in stark contrast to other metalized substrates, where surface nanoparticulate morphology can be altered by relatively low temperatures, with subsequent near-field effects on fluorescence signatures. This finding suggests Rh substrates may be of particular value for higher-temperature MEF experiments or indeed used as an autoclavable substrate.

Acknowledgements

The authors acknowledge the IoF, the department of Chemistry and Biochemistry and UMBC for salary support.

References

- R. R. Chance, A. H. Miller, A. Prock and R. Silbey, *J. Chem. Phys.*, 1975, **63**, 1589–1595.
- S. Choi, E. Y. Choi, D. J. Kim, J. H. Kim, T. S. Kim and S. W. Oh, *Clin. Chim. Acta*, 2004, **339**, 147–156.
- M. E. Cullum, L. A. Lininger, S. Z. Schade, S. E. Cope, J. C. Ragain, Jr and L. G. Simonson, *Mil. Med.*, 2003, **168**, 915–921.
- R. S. Davidson and M. M. Hilchenbach, *Photochem. Photobiol.*, 1990, **52**, 431–438.
- H. Andersson, T. Baechi, M. Hoehle and C. Richter, *J. Microsc.*, 1998, **191**, 1–7.
- J. Enderlein, T. Ruckstuhl and S. Seeger, *Appl. Opt.*, 1999, **38**, 724–732.
- Fluorescence Sensors and Biosensors*, ed. R. B. Thompson, CRC Press, Taylor & Francis Group, LLC, Boca Raton, FL, 2006.
- S. Chowdhury, V. Bhethanabotla and R. Sen, *Appl. Phys. Lett.*, 2009, **95**, 131115.
- F. Stefani, K. Vasilev, N. Bocchio, N. Stoyanova and M. Kreiter, *Phys. Rev. Lett.*, 2005, **94**, 023005.
- S. Garrett, L. Smith and W. Barnes, *J. Mod. Opt.*, 2005, **52**, 1105.
- S. Praharaj, S. Ghosh, S. Nath, S. Kundu, S. Panigrahi, S. Basu and T. Pal, *J. Phys. Chem. B*, 2005, **109**, 13166.
- O. Stranik, H. McEvoy, C. McDonagh and B. MacCraith, *Sens. Actuators, B*, 2005, **107**, 148.
- R. Aroca, G. J. Kovacs, C. A. Jennings, R. O. Loutfy and P. S. Vincett, *Langmuir*, 1988, **4**, 518–521.
- Y. Chen, K. Munechika and D. S. Ginger, *Nano Lett.*, 2007, **7**, 690–696.
- P. P. Cheng, D. Silvester, G. Wang, G. Kalyuzhny, A. Douglas and R. W. Murray, *J. Phys. Chem. B*, 2006, **110**, 4637–4644.
- A. C. Croce, A. Ferrigno, M. Vairetti, R. Bertone, I. Freitas and G. Bottiroli, *Photochem. Photobiol. Sci.*, 2004, **3**, 920–926.
- A. Doron, E. Katz and I. Willner, *Langmuir*, 1995, **11**, 1313–1317.
- M. Kawasaki and S. Mine, *J. Phys. Chem. B*, 2005, **109**, 17254–17261.
- J. Malicka, I. Gryczynski, C. D. Geddes and J. R. Lakowicz, *J. Biomed. Opt.*, 2003, **8**, 472–478.
- J. Dostalek and W. Knoll, *Biointerphases*, 2008, **3**, FD12.
- Theory of Fluorophore–Metallic Surface Interactions*, ed. J. I. Gersten, Springer, New York, 2004.
- A. Kasry and W. Knoll, *Appl. Phys. Lett.*, 2006, **89**, 101106.
- C. D. Geddes and J. R. Lakowicz, *J. Fluoresc.*, 2002, **12**, 121–129.
- K. Aslan, J. R. Lakowicz, H. Szmanski and C. D. Geddes, *J. Fluoresc.*, 2004, **14**, 677–679.
- K. Aslan, R. Badugu, J. R. Lakowicz and C. D. Geddes, *J. Fluoresc.*, 2005, **15**, 99–104.
- K. Aslan, P. Holley and C. D. Geddes, *J. Mater. Chem.*, 2006, **16**, 2846–2852.
- K. Aslan, S. N. Malyn and C. D. Geddes, *Analyst*, 2007, **132**, 1112–1121.
- K. Aslan, S. N. Malyn and C. D. Geddes, *J. Fluoresc.*, 2006, **17**, 7–13.
- Y. Zhang, K. Aslan, M. J. R. Previte and C. D. Geddes, *Appl. Phys. Lett.*, 2007, **90**, 173116.
- K. Aslan, M. J. R. Previte, Y. Zhang and C. D. Geddes, *J. Phys. Chem. C*, 2008, **112**, 18368–18375.
- R. Pribik, K. Aslan, Y. Zhang and C. D. Geddes, *J. Phys. Chem. C*, 2008, **112**, 17969–17973.
- Y. Zhang, A. Padhyay, J. Sevilleja, R. L. Guerrant and C. D. Geddes, *J. Phys. Chem. C*, 2010, **114**, 7575–7581.
- Y. Zhang, A. Dragan and C. D. Geddes, *J. Appl. Phys.*, 2010, **107**, 024302.
- K. Aslan, Z. Leonenko, J. R. Lakowicz and C. D. Geddes, *J. Fluoresc.*, 2005, **15**, 643–654.
- J.-P. Lu, P. W. Chu and R. Raj, *Thin Solid Films*, 1992, **208**, 172–176.
- A. Taflove and S. C. Hagness, *Computational Electrodynamics: The Finite-Difference Time-Domain Method*, Artech House, Norwood, MA, 2000.
- V. Anantha and A. Taflove, *IEEE Trans. Antennas Propag.*, 2002, **50**, 1337–1349.
- K. Aslan, Y. X. Zhang and C. D. Geddes, *J. Appl. Phys.*, 2008, **103**, 084307.
- Y. Zhang, A. Dragan and C. D. Geddes, *J. Phys. Chem. C*, 2009, **113**, 12095–12100.
- Metal-Enhanced Fluorescence*, ed. C. D. Geddes, John Wiley and Sons, New Jersey, 2010, ISBN: 978-0-470-22838-8.
- M. H. Chowdhury, K. Aslan, S. N. Malyn, J. R. Lakowicz and C. D. Geddes, *J. Fluoresc.*, 2006, **16**, 295–299.
- M. H. Chowdhury, K. Aslan, S. N. Malyn, J. R. Lakowicz and C. D. Geddes, *Appl. Phys. Lett.*, 2006, **88**, 173104.